Arginine-induced conformational change in the c-ring/a-subunit interface of ATP synthase

Thomas Vorburger[1], Judith Zingg Ebneter[1], Alexander Wiedenmann[1], Damien Morger[1], Gerald Weber[1], Kay Diederichs[2], Peter Dimroth[1] and Christoph von Ballmoos[1]

1 Institut für Mikrobiologie, ETH Zürich Hönggerberg, Switzerland
2 Fachbereich Biologie, Universität Konstanz M656, Germany

The rotational mechanism of ATP synthases requires a unique interface between the stator a subunit and the rotating c-ring to accommodate stability and smooth rotation simultaneously. The recently published c-ring crystal structure of the ATP synthase of *Ilyobacter tartaricus* represents the conformation in the absence of subunit a. However, in order to understand the dynamic structural processes during ion translocation, studies in the presence of subunit a are required. Here, by intersubunit Cys–Cys cross-linking, the relative topography of the interacting helical faces of subunits a and c from the *I. tartaricus* ATP synthase has been mapped. According to these data, the essential stator arginine (aR226) is located between the c-ring binding pocket and the cytoplasm. Furthermore, the spatially vicinal residues cT67C and cG68C in the isolated c-ring structure yielded largely asymmetric cross-linking products with aN230C of subunit a, suggesting a small, but significant conformational change of binding-site residues upon contact with subunit a. The conformational change was dependent on the positive charge of the stator arginine or the aR226H substitution. Energy-minimization calculations revealed possible modes for the interaction between the stator arginine and the c-ring. These biochemical results and structural restraints support a model in which the stator arginine operates as a pendulum, moving in and out of the binding pocket as the c-ring rotates along the interface with subunit a. This mechanism allows efficient interaction between subunit a and the c-ring and simultaneously allows almost frictionless movement against each other.

F_1F_0 ATP synthases are responsible for production of the majority of ATP, the universal energy currency in every living organism. These enzymes synthesize ATP from ADP and inorganic phosphate by a rotary mechanism, utilizing the electrochemical gradient provided by oxidative phosphorylation, decarboxylation phosphorylation or photophosphorylation. The vast majority of F-ATPases use protons as their coupling ions, but those of some anaerobic bacteria use Na^+ ions instead. The enzyme can be divided into two domains, each capable of acting as an independent motor. In bacterial systems, the catalytic F_1 domain, consisting of subunits $\alpha_3\beta_3\gamma\delta\epsilon$, is connected to the membrane-embedded F_0 domain via two stalks. The F_0 domain consists of one a subunit, two b subunits and 10–15 c subunits, depending on the organism [1]. During ATP synthesis, the flux of H^+ or Na^+ through F_0 following the electrochemical potential is used to drive rotation of the c-ring relative to the stator subunits $ab_2\delta\alpha_3\beta_3$. This rotational torque applied to the central

stalk, consisting of subunits γ and ε, drives the conformational changes in the catalytic F_1 part, enabling ATP synthesis [2,3].

During ATP synthesis, it is envisaged that coupling ions enter the F_0 part from the periplasm through an aqueous pathway located within subunit *a*, and are bound to the appropriately positioned binding sites on the rotating *c*-ring. From there, they are released into the cytoplasmic reservoir through a poorly understood pathway [3]. Although subunits *a* and *c* most likely provide exclusively the required features for the ion pathway, Na^+ or H^+ translocation across the membrane is only observed in the presence of subunit *b* [4,5]. The high-resolution structures of the isolated Na^+-binding *c*-ring from *Ilyobacter tartaricus* and the *K*-ring from *Enterococcus hirae* revealed precisely how the Na^+ ion is stably coordinated within binding sites outside the *a/c* interface [6,7]. However, ion loading and unloading of these binding sites from or towards either reservoir requires the presence of subunit *a* [8,9]. It is therefore important to investigate the dynamic structural changes in the *c* subunits that are in contact with subunit *a*.

Efforts to understand the interaction between subunit *a* and the *c*-ring were made several years ago by Fillingame *et al.* They presented an elaborate study on the interacting helical faces of subunits *a* and *c* of *Escherichia coli* ATPase using disulfide cross-linking [10]. Based on NMR structures of the monomeric *c* subunit in organic solvent mixtures at various pH values, a mechanism for ion translocation in F_0 was proposed, which involves swiveling of the outer helix of subunit *c* by 180° to be congruent with both biochemical and structural data [11,12]. The recently published crystal structure of the *I. tartaricus* *c*-ring and an *E. coli* *c*-ring homology model revealed that such a large conformational change is unlikely, as all residues on the *c*-ring, which were found to form disulfide bridges with subunit *a*, are facing outwards [6]. Large conformational changes were not found in NMR studies of the *c*-monomer of the H^+-translocating ATP synthase of *Bacillus* PS3 in organic solvents over a broad pH range (pH 2–8) [13]. Very recently, Fillingame *et al.* retreated from their swiveling model. They propose that such a twinned conformation of the *c*-subunit is indeed found in membranes, but does not necessarily contribute to the mechanism of ion translocation [14].

In the present study, we engineered various cysteine mutants within subunits *a* and *c* of *I. tartaricus* ATP synthase, and quantified the formation of *ac* complexes by disulfide cross-linking. We provide experimental evidence for a small but significant conformational change within the structure of the ion-binding site upon contact with subunit *a*. This conformational change is dependent on the presence of the conserved arginine in the stator. These results are supported by energy-minimization calculations of the interaction between the stator arginine and the *c*-ring, and suggest a general molecular model for rotation of subunit *c* against subunit *a*.

Throughout the paper, the cytoplasmic and periplasmic reservoirs are denoted as *N*-side and *P*-side, respectively.

Results

Based on suppressor mutations, helix 4 of subunit *a*, containing the universally conserved arginine, was proposed to interact closely with the *c*-ring [15]. This finding was corroborated by a detailed study of Cys–Cys cross-link formation between residues of helix 4 from subunit *a* and those of helix 2 from subunit *c* [10].

In the present study, we investigate by similar means the interaction between interfacial helices of subunits *a* and *c* in the *I. tartaricus* enzyme, and reconcile this data with newly available structural and functional knowledge of the *c*-ring.

Characterization of the *a/c* interface by cysteine cross-linking experiments

Cell membranes, containing combined cysteine substitutions in helices 4 and 2 of subunits *a* and *c*, respectively, were isolated under reducing conditions and subjected to copper phenanthroline-mediated oxidation as described in Experimental procedures. Due to the low expression levels of the recombinant Na^+-translocating ATP synthases, we enriched hydrophobic proteins, including subunit *a* and *c* and their cross-linking products, by organic extraction under acidic conditions as described in Experimental procedures. This process is highly reproducible and did not increase the variance in our experiments. The formation of cross-linking products was analyzed by SDS–PAGE and immunoblotting using antibodies against subunits *a* and *c*. Cross-linking products containing subunits *a* and *c* were identified by reaction with both antibodies (Fig. 1A). Immunoblots against subunit *a* were routinely used for quantification as indicated in Fig. 1B. Immunoblots against subunit *c* produced similar results, but their quantification was less accurate due to the large excess of subunit *c* monomer compared with *ac* cross-linking products. Appropriate control experiments were performed. If the reaction was stopped using *N*-ethylmaleimide (NEM) and EDTA prior to incubation with copper-(1,10-phenanthroline)$_2$SO$_4$ (CuP), no formation of cross-linking
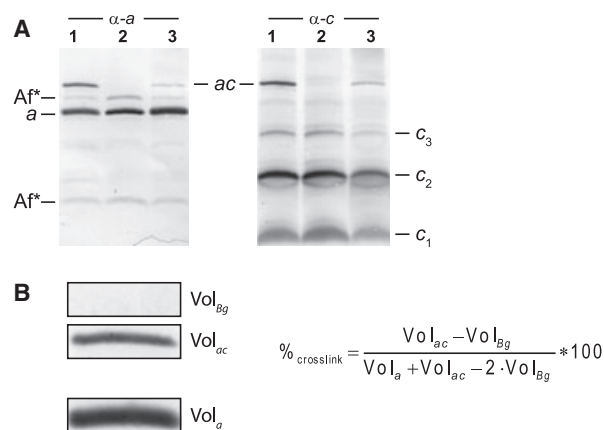
Fig. 1. (A) Identification of *ac* cross-linking products by western blot analysis and antibody detection. Membranes were oxidized using CuP for 1 h at room temperature and subunits *a* and *c* were extracted using chloroform/methanol. After electrophoresis under non-reducing conditions, proteins were transferred to nitrocellulose membranes and visualized by immunoblotting. Antibodies against subunit *a* (left panel) and subunit *c* (right panel) were utilized to identify the *ac* cross-linking products. Bands marked Af* are artifacts from DK8 that are not related to the ATP synthase. Shown is a representative analysis of *c*T67C/*a*N230C (lane 1), *c*T67C (lane 2) and *c*G68C/*a*N230C mutants (lane 3). (B) Quantification of *ac* cross-link formation in subunit *a* immunoblots. Immunoblots were scanned and the bands corresponding to subunit *a* and to the cross-linking product *ac* were quantified and expressed as volumes (Vol$_a$ and Vol$_{ac}$) using QUANTITY ONE software. For every blot, a background volume (Vol$_{Bg}$) was calculated from three individual squares. The amount of cross-link formation was then calculated according to the equation shown.

products was observed (data not shown). Likewise, SDS–PAGE under reducing conditions to break disulfide bonds indicated that no cross-linking products were formed (data not shown).

In a first series of experiments, 16 cysteine pairs were constructed and the amount of intersubunit cross-link formation was quantified (Table 1). Overall, we found cross-linking yields of up to 50%, comparable to the study by Jiang and Fillingame [10]. Ten pairs yielded substantial amounts of *ac* cross-linking products (> 18%), whereas the remaining mutants yielded only little or no cross-linking products. Table 2 shows the separation of these mutants into five categories with respect to their *ac* cross-linking yields. When these data were compared with cross-linking data for the *E. coli* enzyme, six of the corresponding Cys pairs produced *ac* cross-linking products to a comparable extent. For four of the mutant pairs, the tendency to form *ac* cross-links deviated significantly between the *I. tartaricus* enzyme and the *E. coli* enzyme. Finally, for three *I. tartaricus*

Cys–Cys double mutants, no data was available regarding the *E. coli* homologues. As would have been predicted from the crystal structure for the *I. tartaricus* *c*-ring and the homology model for the *E. coli* *c*-ring [6], the strongest cross-linking yields were obtained with residues facing towards the outside in the *c*-ring structures, reinforcing the notion that no major conformational change takes place in the *c*-ring structure upon entry into the *a/c* interface.

Taken together, overall similar *ac* cross-linking patterns are found in the enzymes of *I. tartaricus* and *E. coli* (Fig. 2A,B), albeit with significantly different yields between some of the corresponding pairs. These differences imply that a direct comparison of *c*-ring structures based on their primary amino acid sequences is difficult. It is likely that the majority of the *c*-ring residues are involved in overall organization and stability of the *c*-ring to provide a scaffold for a few functionally important residues.

Replacement of the conserved *a*R226 by uncharged residues changes the cross-linking pattern

In the crystal structure of the *c*-ring, the spatial localization of residues *c*T67 and *c*G68 from two adjacent helices of the binding pocket is very similar, and, when substituted by cysteine, their distances to *a*N230C are likely to be almost identical (Fig. 2C,D). In the absence of any driving force, the ATP synthase is in its idling mode, performing back-and-forth rotations within a narrow angle, which allows Na$^+$ exchange across the membrane [16,17]. These movements ensure that residues *c*T67C and *c*G68C are accessible for cross-link formation by *a*N230C from any angle. This scenario predicts that *c*T67C and *c*G68C form similar amounts of cross-linking products with *a*N230C. Experimentally, however, about 25% cross-linking product formation was found in the *c*T67C mutant, whereas only very low amounts of cross-linking product (< 5%) were observed with the *c*G68C mutant (Fig. 1A, lanes 1 and 3), suggesting a distinct spatial arrangement of these residues in the *a/c* interface compared to the crystal structure.

The different spatial orientation of these two *c*-ring residues within and outside of the interface with subunit *a* might be elicited by electrostatic interactions between the binding site and the stator arginine. Therefore, in subsequent experiments, the stator *a*R226 was replaced by either A, H, Q or S to yield the triple mutants *a*R226X/*a*N230C/*c*T67C and *a*R226X/*a*N230C/*c*G68C (X = A, H, Q or S, respectively). The

Table 1. Relative yield of *ac* cross-linking products between cysteines introduced in subunits *a* and *c* at the positions indicated. The developed immunoblots were scanned and bands corresponding to *ac* and *a* were quantified. The relative yield of *ac* cross-linking products was calculated as shown in Fig 1B, and 100% cross-linking would therefore correspond to the presence of the entire subunit *a* in the form of *ac* cross-linking products. At least three individual measurements (new protein expression) were performed to determine product formation.

Cys pair	Relative yield of *ac* cross-linking product (%)
*a*I223C/*c*V58C	46.9 ± 4.6
*a*I223C/*c*L59C	37.4 ± 4.5
*a*N230C/*c*S66C	37.7 ± 6.3
*a*N230C/*c*T67C	25.4 ± 6.7
*a*N230C/*c*G68C	4.8 ± 1.8
*a*N230C/*c*I69C	23.9 ± 5.9
*a*N230C/*c*Y70C	30.3 ± 7.1
*a*A233C/*c*I69C	8.6 ± 2.6
*a*A233C/*c*Y70C	36.4 ± 2.4
*a*I237C/*c*V73C	23.6 ± 6.6
*a*G239C/*c*L76C	7.1 ± 3.7
*a*G239C/*c*I77C	2.3 ± 2.1
*a*L240C/*c*L76C	18.2 ± 4.4
*a*L240C/*c*I77C	4.1 ± 3.2
*a*L241C/*c*L76C	21.4 ± 2.3
*a*L241C/*c*I77C	6.0 ± 1.3

Table 2. Comparison between *ac* cross-link formation using cysteine mutants in the *a/c* interface of the *E. coli* and *I. tartaricus* ATP synthases. Corresponding cross-linking products are shown in the same row and relative cross-linking yields have been characterized as follows: ±, < 5%; +, 6–10%; ++, 11–20%; +++, 21–40%; ++++, > 40%. ND, not determined.

| *I. tartaricus* ATPase		*E. coli* ATPase [10]	
Cys pair (*I. t.* numbering)		Cys pair (*E. c.* numbering)	
*a*I223C/*c*V58C	++++	*a*L207C/*c*F54C	+
*a*I223C/*c*L59C	+++	*a*L207C/*c*I55C	++
*a*N230C/*c*S66C	+++	*a*N214C/*c*A62C	+++
*a*N230C/*c*T67C	+++	*a*N214C/*c*I63C	ND
*a*N230C/*c*G68C	±	*a*N214C/*c*P64C	ND
*a*N230C/*c*I69C	+++	*a*N214C/*c*M65C	+++
*a*N230C/*c*Y70C	+++	*a*N214C/*c*I66C	+
*a*A233C/*c*I69C	+	*a*A217C/*c*M65C	±
*a*A233C/*c*Y70C	+++	*a*A217C/*c*I66C	±
*a*I237C/*c*V73C	+++	*a*I221C/*c*G69C	+++
*a*G239C/*c*L76C	+	*a*I223C/*c*L72C	+++
*a*G239C/*c*I77C	±	*a*I223C/*c*Y73C	ND
*a*L240C/*c*L76C	++	*a*L224C/*c*L72C	+
*a*L240C/*c*I77C	±	*a*L224C/*c*Y73C	++++
*a*L241C/*c*L76C	+++	*a*L225C/*c*L72C	+
*a*L241C/*c*I77C	+	*a*L225C/*c*Y73C	+++
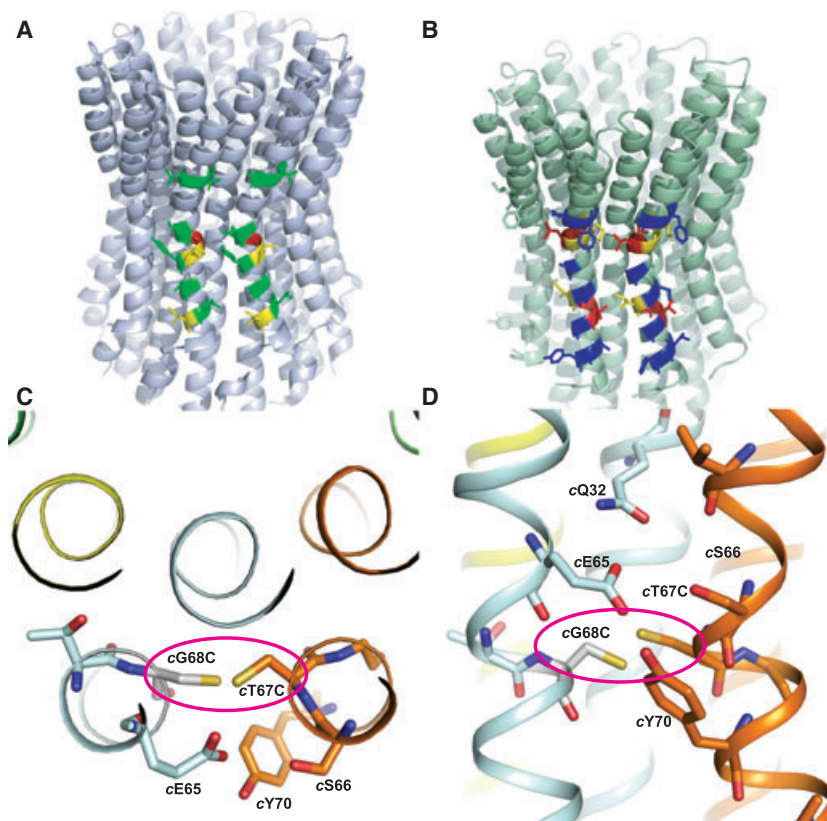
Fig. 2. (A) Location of cross-links in the *I. tartaricus a/c* interface found in this study. Green (good yield), yellow (medium yield), red (minor or no yield). (B) Location of cross-links in the *E. coli a/c* interface [10]. Blue (good yield), yellow (medium yield), red (minor or no yield). (C) Top view into the binding pocket of the *I. tartaricus c*-ring. Residues 67 and 68 are mutated to cysteines to illustrate their almost identical location within the binding site. (D) Side view into the binding pocket of the *I. tartaricus c*-ring. Residues 67 and 68 are mutated to cysteines to illustrate their almost identical position within the membrane bilayer. All images were prepared using PYMOL (DeLano Scientific).
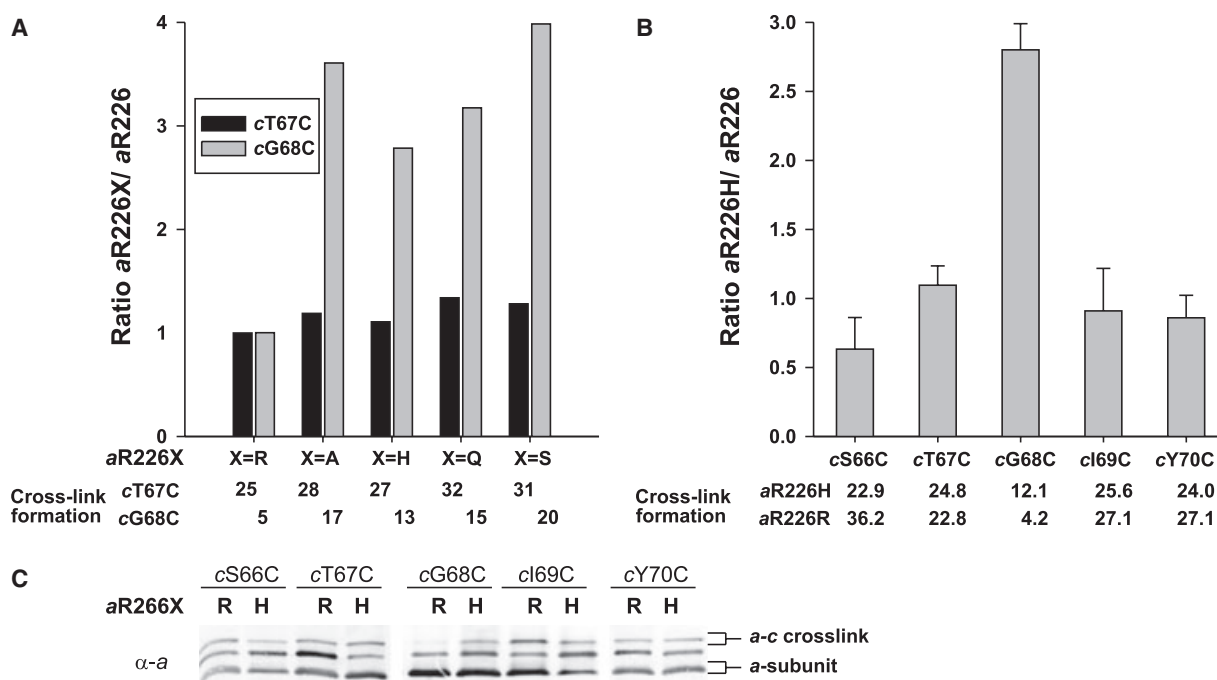
Fig. 3. (A) Effect of *a*R226X mutations on formation of Cys–Cys cross-linking products between *a*N230C and *c*T67C or *c*G68C, respectively. The values shown are the ratios of cross-linking product formation between *a*N230C and *c*T67C or *c*G68C, respectively, in the R226X background versus those in the wild-type background. Details are given in Fig. 1 and Experimental procedures. CuP-catalyzed air oxidation of the membranes was carried out at pH 8. The numbers below the figure are the average (mean) yields of *ac* cross-link formation (as a percentage of the total amount of *a* subunit). (B) Formation of *ac* cross-linking products between *a*N230C and mutants *c*S66C, *c*T67C, *c*G68C, *c*I69C and *c*Y70C in the presence or absence of the *a*R226H replacement. The values shown are the ratios between the triple and the double mutants. The absolute cross-link formation yields (mean) are shown below. (C) Western blot analysis using antibodies against subunit *a* for the experiment described in (B).

results for relative cross-linking product formation (compared to X = R) for these triple mutants are shown in Fig. 3A. For the *a*N230C/*c*G68C cysteine pair, the yield of cross-linking products for all *a*R226X substitutions was significantly increased (up to 20%) compared to the wild-type background. On the other hand, the *a*R226X substitution did not significantly affect cross-link formation by the *a*N230C/*c*T67C cysteine pair.

To further investigate the influence of the stator arginine on the conformational changes of the *c* subunit, the amounts of cross-link formation between *a*N230C and cysteine mutants of subunit *c* around the binding site (residues 66–70) in the wild-type and *a*R226H background were compared. The results in Fig. 3B,C indicate that the *a*R226H substitution decreased the amount of cross-link formation by the pair *a*N230C/*c*S66C to about 70% of that of the wild-type, while that for the *a*N230C/*c*G68C pair increased about 280%, and that for the pairs *a*N230C/*c*T67C, *a*N230C/*c*I69C and *a*N230C/*c*Y70C was not significantly affected.

Cross-linking product formation by *a*N230C/ *c*G68C is influenced by the protonation state of histidine in *a*R226H

To elucidate whether the altered side chains themselves or the presence or absence of a positive charge within the *a*/*c* interface is responsible for the amount of *ac* cross-link formation, we took advantage of the fact that the protonation state of a histidine residue can be changed in the near-neutral range [pK_a(His) = 6.0]. The experiments described above were repeated at pH 5 and 6 in order to protonate the histidine in *a*R226H. To control the influence of the pH on the formation of Cys–Cys cross-linking products, we included control experiments at both acidic pH values in which the arginine at position 226 was not changed.

The results of these measurements (Fig. 4A) show the amounts of cross-link formation at the various pH values normalized to the amounts at pH 5. In the control reactions in the presence of *a*R226, labeling at pH 6 and 8 was increased approximately 2.5-fold and 4-fold, respectively, compared to pH 5, reflecting the
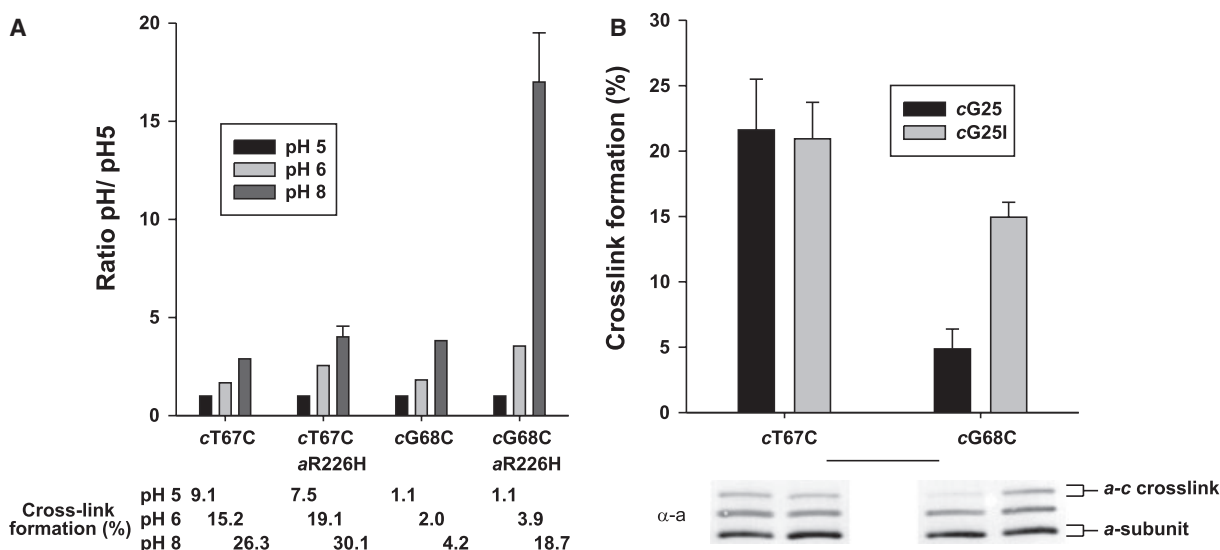
Fig. 4. (A) pH dependence of cross-link formation between *a*N230C and *c*T67C or *c*G68C, respectively, in the wild-type or *a*R226H background. Membranes containing the mutant proteins were exposed to CuP at pH 5, 6 and 8, and the relative yields of *ac* cross-linking products were determined. The values shown are the ratios of cross-link yields at the pH indicated to the yields at pH 5, to illustrate the influence of pH on cross-link formation. The absolute cross-link formation yields (means) are displayed below the figure. If three or more experiments were performed, error bars are indicated. (B) Influence of *c*G25I on formation of cross-linking products. Yields of *ac* cross-linking products for the two Cys–Cys pairs *a*N230C/*c*T67C and *a*N230C/*c*G68C in the presence or absence of the *c*G25I mutation at pH 8 are shown. The corresponding western blot analysis using antibodies against subunit *a* is shown below.

pH dependence of the disulfide formation reaction. In the *a*R226H/*a*N230C/*c*T67C mutant, comparable values were obtained. In the *a*R226H/*a*N230C/*c*G68C mutant, however, the same measurements resulted in a 4-fold (pH 6) and 17-fold (pH 8) increased cross-link formation. These results show that formation of the *a*N230C/*c*G68C cross-linking products is severely diminished in presence of a positively charged amino acid at position 226 of the *a* subunit, i.e. either the wild-type (*a*R226) or the protonated form of the *a*R226H mutant.

Effect of the *c*G25I mutation on cross-link formation between *a*N230C and *c*T67C or *c*G68C, respectively

The various amounts of cross-link formation in the presence or absence of a positive charge might result from a partial helical rotation due to electrostatic interactions between the stator charge and the abutting rotor site. Likewise, several side chains from the binding site might be significantly rearranged upon contact with the stator charge on subunit *a* (see Discussion). Both kinds of structural changes are preferred as the helix packing between inner and outer helices is not tight in this region due to the absent side chain of *c*G25 on the inner helices. Although residue *c*G25 is

conserved in Na$^+$-translocating ATP synthases, it does not belong to the G-X-G-X-G-X-G motif responsible for the tight packing between the inner helices [18]. Replacement of the small glycine by a bulky isoleucine residue might occupy the space needed for the conformational changes envisaged above. We therefore determined the yield of *a*N230C/*c*T67C and *a*N230C/*c*G68C cross-linking products in the presence and absence of the *c*G25I substitution. Importantly, the *c*G25I mutation did not disturb the assembly of an oligomeric *c*-ring as judged by SDS–PAGE after purification of the enzyme (data not shown). As shown in Fig. 4B, the *c*G25I replacement had only little effect on the formation of cross-linking products by the *a*N230C/*c*T67C cysteine pair but increased that of the *a*N230C/*c*G68C pair about 3-fold over the wild-type (*c*G25) control.

ATP synthesis measurements with single mutants *c*G25I, *c*T67C and *c*G68C

We wished to determine whether the effect of the *c*G25I mutation on cross-link formation is reflected by functional enzyme studies. For this reason, mutants *c*G25I, *c*T67C, *c*G68C and the recombinant wild-type enzyme were purified, reconstituted into proteoliposomes and tested for ATP synthesis activity
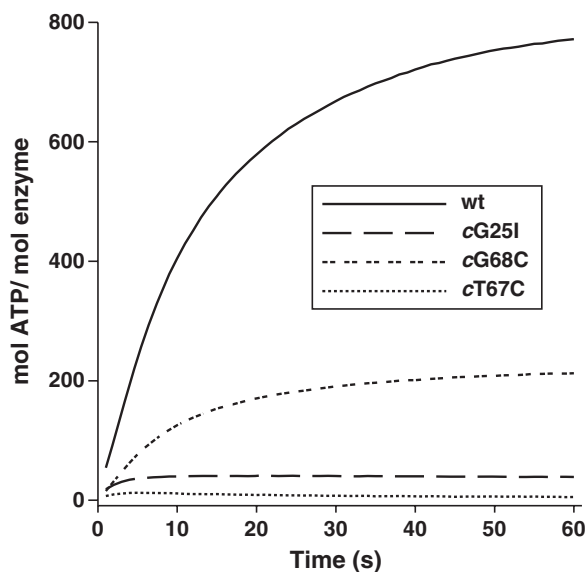
Fig. 5. ATP synthase activities in the wild-type *I. tartaricus* ATP synthase and *c* subunit mutants. The purified enzymes were reconstituted into proteoliposomes and the synthesis of ATP was followed after application of a K^+/valinomycin diffusion potential. In control experiments, the membrane potential was dissipated by addition of the K^+/H^+ exchanger nigericin, and the values obtained by these measurements were subtracted. The luminescence time traces of representative experiments for the wild-type and indicated mutant enzymes are shown. The rates of ATP synthesis were calculated under the assumption that 100% of ATP synthase molecules were incorporated into the liposomes during the reconstitution process.

after energization by a K^+/valinomycin-induced diffusion potential (positive inside). Maximal enzyme activity was observed in the wild-type enzyme, but mutant *c*G68C also showed a substantial synthesis rate (about 30% of wild-type) (Fig. 5). No significant ATP synthesis was observed in the *c*G25I mutant, emphasizing the functional importance of the small glycine residue. Likewise, we were not able to detect any activity in the *c*T67C mutant, indicating the physiological importance of threonine at position 67.

Energy-minimization calculations for interaction of *a*R226 with the *c*-ring

To further probe critical interactions in the *a/c* interface, energy-minimization calculations for interaction between a seven amino acid stretch of subunit *a* (*a*I225–*a*M231), containing the conserved residues *a*R226 and *a*N230, and the *c*-ring crystal structure were performed. The minimization consistently adjusted the conformation of *a*I225 to *a*M231 such that the plane of the guanidino group of *a*R226 was

placed optimally in the entrance of the binding pocket of the *c*-ring. While full mobility (no harmonic restraints) was allowed for the subunit *a* stretch and the side chains of the *c*-ring residues, various degrees of motional freedom were applied to the backbone of the *c*-ring helices using harmonic restraints (10 kcal·mol^{-1} Å^2). The resulting conformation of *a*R226 after energy minimization was found to be insensitive to the exact starting conformation applied, and visually identified hydrogen-bond patterns indicated a possible mode of interaction between *a*R226 and the binding pocket. The detailed results of these calculations are discussed below.

Discussion

A stator charge-induced conformational change within the binding pocket

Elucidation of the high-resolution structures of the Na^+-dependent rotor rings of *I. tartaricus* F-ATP synthase and *E. hirae* V-ATPase represents a significant step towards a mechanistic understanding of ion translocation in these enzymes [6,7]. In the *I. tartaricus* structure, the ion-binding pocket is located close to the outer surface of the *c*-ring, but is shielded from the hydrophobic environment by the side chains of *c*E65, *c*S66 and *c*Y70. The side chain of *c*Y70 is not directly involved in Na^+ coordination, but forms a hydrogen bond to the conserved *c*E65 that stabilizes the overall shape of the binding pocket. In this conformation, the aromatic side chain seems to be ideally suited to shield the polar binding pocket from the lipid bilayer. The significance of the phenolic group of *c*Y70 for stability of the binding site has been demonstrated by an about 30-fold decrease in Na^+ binding affinity in the *c*Y70F mutant [19].

Electrostatic interactions between the binding site and the stator arginine have been proposed to discharge the ion in the subunit *a/c* interface, and this hypothesis has been experimentally verified [5]. In this study, we wished to determine whether a conformational change within the binding pocket, induced by the positive stator charge, provides a molecular rationale for dislodging of the ion, and probed the distances between *c*-ring residues near the binding site and helix 4 of subunit *a* by Cys–Cys cross-linking experiments. Notably, the *a*N230C residue, which is located one helical turn towards the *P*-side of the stator arginine, formed substantially fewer cross-linking products with *c*G68C than with *c*T67C, although both side chains adopt a very similar position in the structure of the isolated *c*-ring. These data indicate

that *c*G68 is shielded or displaced from helix 4 of subunit *a* in the subunit *a/c* interface. Factors eliciting the corresponding conformational change at the ion-binding site could thus be monitored by comparing cross-linking yields between *a*N230C and *c*T67C or *c*G68C. Importantly, upon replacement of the stator arginine by electroneutral amino acids, formation of cross-linking products between *a*N230C and *c*G68C was specifically augmented, while those with *c*T67C, *c*I69C or *c*Y70C were not affected. Hence, the stator arginine appears to elicit a distinct conformational change in the *c* subunit binding site without affecting the global conformation of the *c*-ring. These conclusions were corroborated by comparing cross-link formation in the *a*R226H background under various protonation states of the histidine. At low pH, when the histidine is protonated, the cross-linking pattern resembles that in the presence of arginine. At higher pH, however, when the histidine is expected to be neutral, the pattern resembled that in the *a*R226A or *a*R226S mutants. A similar effect of pH to that observed in cross-linking experiments with the *a*R226H mutant was also found in ATP-driven Na$^+$ transport and Na$^+$ exchange experiments with this mutant [5].

Is it possible to envisage molecular details of this conformational change on the basis of the *c*-ring structure? Swiveling of part of the outer helix of subunit *c* (containing *c*E65 and *c*G68) would be one possibility for bringing the *c*T67C and *c*G68C residues into unequal positions with respect to *a*N230C. It is also conceivable that side-chain movements of several residues in the presence of the stator charge would induce a new energetically favorable conformation that blocks access to the *c*G68C residue. Previously, the stator charge was thought to interact electrostatically with the acidic side chain of the ion binding glutamate, initiating a large side-chain movement (opposite to the direction of rotation) that opens the binding site [6,7]. In this scenario, residue *c*G68C (which is on the same helix as the rotated *c*E65) would become further exposed and not shielded from contact with subunit *a* as observed in our present experiments. Upon helical rotation in the opposite direction as proposed above, however, *c*G68C would be disconnected from the interface, and cross-link formation would be impeded. We reasoned that the rotating part of the helix is most likely distal to *c*V63, where the helix is broken because the backbone carbonyl of *c*V63 is involved in Na$^+$ coordination. It is interesting to note that *c*G68 is positioned opposite another glycine (*c*G25) on the inner helix. The space provided by the absence of side chains would allow a helical segment around *c*G68 to

rotate towards the inner helices (Fig. 6A). A similar cavity is formed by glycines 27 and 66 in the K-ring of *E. hirae* [7]. If this hypothesis is valid, the conformational change should be obstructed by replacement of the glycine on the inner helix by a more bulky residue. Indeed, in the *c*G25I mutant, a significantly increased amount of cross-link formation with *c*G68C was observed, indicating that the bulky side chain prevented the conformational change in the rotor/stator interface. The functional importance of *c*G25 is underlined by ATP synthesis measurements – no detectable ATP formation was observed in the *c*G25I mutant. Instead of helical rotation, it is also feasible that interaction with the stator charge pushes part of the helix containing *c*G68 and *c*E65 towards the center of the *c*-ring. Likewise, the cavity formed by glycines *c*G68 and *c*G25 might accommodate this helical motion.

Energy-minimization calculations support the proposed conformational change

The data reported in this study allowed us to produce a model of the interacting helical faces of subunit *a* and the *c*-ring. As significant cross-link formation with *a*N230C was found with residues 66–70 of the *c*-ring, it was assumed that the position of the *a*N230C residue is directly opposite the binding site. This suggestion was corroborated by strong cross-link formation between *a*A233C and *c*Y70C, but only weak cross-link formation between *a*A233C and *c*I69C. This positions the relative height of *c*Y70 between residues *a*N230 and *a*A233. These considerations indicate that the stator arginine is clearly shifted towards the *N*-side with respect to the binding site. Consequently, the long side chain from *a*R226 reaches the binding site from the *N*-side by perfectly fitting the curved surface of the hourglass shape of the *c*-ring. Such an interaction of the arginine with the binding site allows close contact of the two subunits and should also serve as an efficient seal to prohibit ions arriving from the periplasm from escaping to the cytoplasm.

In order to gain insight into the interaction of the stator arginine with the binding site, we modeled a stretch of seven amino acids of helix 4 of subunit *a* into the *c*-ring structure and computationally minimized the energy of this assembly. Depending on the applied parameters, two possible coordinations of the arginine within the binding pocket were obtained. The binding of the arginine is stabilized by a number of hydrogen bonds to the Na$^+$-binding ligands (oxygen atoms of *c*E65, *c*V63 and *c*Q32). These hydrogen bonds minimize the polarity of the arginine in the hydrophobic environment of the *a/c* interface within

Fig. 6. (A) Perspective view of the surface of the *c*-ring of *I. tartaricus*. The atom boundaries are displayed as surfaces to visualize the cavity at the *P*-side of the ion-binding site. The residues of the ion-binding site and the glycine residues *c*G25 and *c*G68 around the cavity are also shown. (B) Side-chain movements observed after energy-minimization calculations for the *c*-ring and a heptapeptide of helix 4 of subunit *a*. The calculated positions of the binding-site residues in the presence (light blue) or absence (light pink) of harmonic backbone restraints of the outer helices are shown with respect to the crystal structure (green) used as the starting point for the calculations. Red, oxygen; blue, nitrogen. (C,D) Coordination of the stator arginine after energy-minimization calculations for the *c*-ring and a heptapeptide of helix 4 of subunit *a*. The calculated positions and possible hydrogen bonds of the binding-site residues on the *c*-ring and the stator arginine in the presence (C) or absence (D) of harmonic backbone restraints of the outer helices are shown. Putative hydrogen bond lengths are marked in Å. All images were prepared using PYMOL (DeLano Scientific).
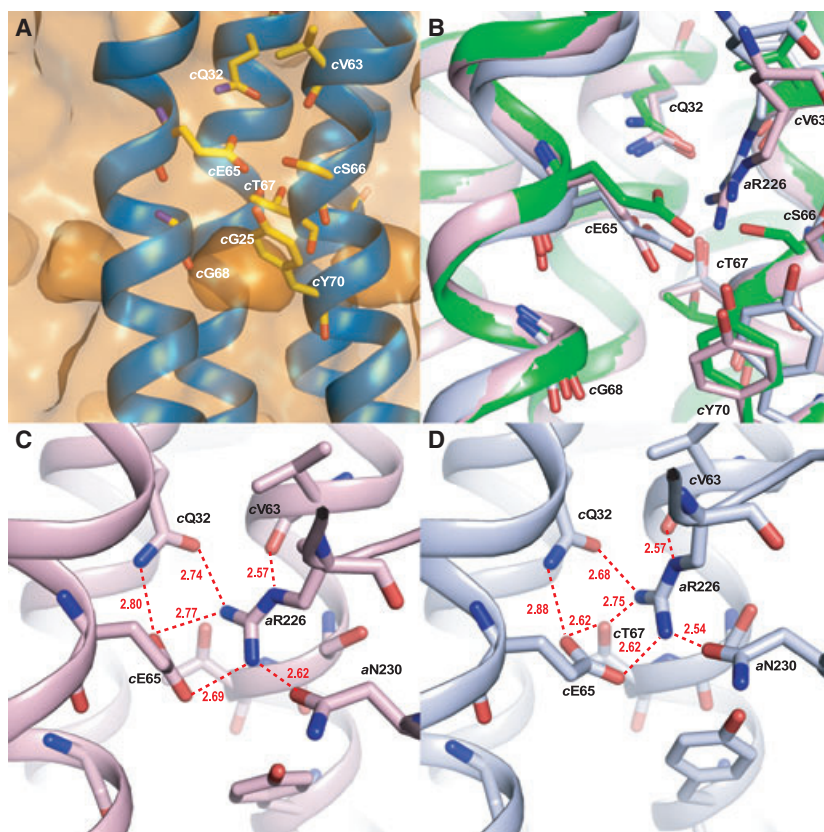
the membrane. In all calculations, a hydrogen bond was formed between the γNH group and the backbone oxygen of *c*V63, guiding the arginine side chain downwards into the binding pocket. In Fig. 6C,D, two conformations of arginine coordination are depicted. In Fig. 6C, movement of the backbone was restricted within harmonic restraints, and therefore only side-chain movements are observed. As expected, the arginine is able to form four hydrogen bonds with *c*Q32, *c*V63 and *c*E65. Another hydrogen bond is formed with *a*N230 of subunit *a*. In Fig. 6D, where no restrictions were imposed on the backbone of the outer rings of helices, a different coordination of the arginine was obtained. Again, *c*Q32, *c*V63, *c*E65 and *a*N230 formed hydrogen bonds with the arginine. However, unlike in the calculation above, only one oxygen atom of *c*E65 was involved in arginine coordination, and the other oxygen formed a hydrogen bond with *c*T67. To allow for this interaction, the side chain of *c*T67 was reoriented, which simultaneously enabled it to form a hydrogen bond with the NH$_2$ group of arginine *a*R226 that reacted with the second oxygen of the glutamate in the first model.

In both calculations, the interaction with the arginine forces the glutamate to move away from its original position towards the cavity formed by *c*G25/*c*G68, as suggested above. Most interestingly, this movement releases the hydrogen bond between *c*E65 and *c*Y70, indicating that the polar arginine uses both oxygens of the glutamate to form hydrogen bonds. Loss of the hydrogen bond between *c*E65 and *c*Y70 allows the side chain of *c*Y70 to accommodate to a new environment, which could be an important step in the ion-translocation mechanism, e.g. by enabling the contact of the periplasmic access pathway with the binding site.

Only a very minor rotation of a helical strip (although in the proposed direction) as suggested above was observed in the calculations; instead there was a shift towards the inner ring of helices, as proposed alternatively. It is not possible, however, to draw direct conclusions from these observations, as important parameters of the native *a/c* interaction were neglected in the energy-minimization calculation (e.g. influence of membrane potential, influence of the peripheral stalk, etc). Nevertheless, the calculation indicates some structural flexibility within the helical strip between the helix break at *c*V63 and the unstructured region around *c*Y80. Such flexibility might permit an efficient *c*-ring rotation when in contact with subunit *a* and accommodate transient structural

changes during loading of Na^+ onto the binding site. Additionally, we performed a simulation in which aR226 was replaced by a histidine. The binding-site residues adopted similar positions as in the calculation with arginine (cE65 pushed towards the cavity, hydrogen bond to c70Y lost), reinforcing our findings from the cross-linking studies (data not shown).

A similar localization of the stator arginine, i.e. slightly shifted towards the N-side with respect to the conserved acidic residue in the c-ring, was also proposed for *E. coli* ATP synthase [10]. It might be that the described interaction of subunits a and c in the *I. tartaricus* enzyme is a general feature of all ATP synthases.

Implications for the ion-translocation mechanism

The Na^+/H^+ antiporter inhibitor ethyl isopropyl amiloride (EIPA) is also known to block Na^+-dependent ATP hydrolysis of the *I. tartaricus* enzyme in a Na^+-dependent manner [20], indicating that EIPA and Na^+ compete for the same binding site (Fig. 7). As the structure of the amiloride derivative mimics that of the stator arginine by combining a positively charged guanidino group with a hydrophobic environment, EIPA is suggested to block the enzyme by occupying the binding
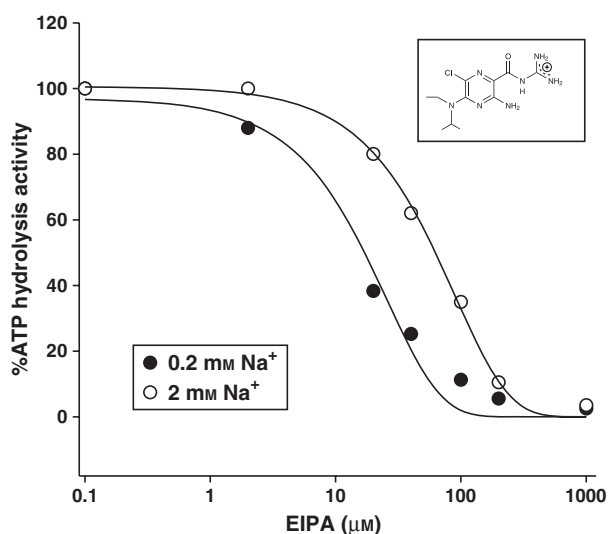

Fig. 7. Inhibition of ATP hydrolysis activity by EIPA. Purified ATP synthase from *I. tartaricus* in the presence of either 0.2 mM NaCl (filled circles) or 2 mM NaCl (open circles) was incubated with various concentrations of EIPA, and ATP hydrolysis rates were determined using the coupled enzyme assay as described previously [30]. Logarithmic scaling of the x axis and exponential decay fitting were applied to illustrate the competition of EIPA and Na^+ for the same binding site. Inset: chemical structure of EIPA.

site. It is of interest that the H^+-translocating enzyme of *E. coli* is not inhibited by EIPA and that this enzyme lacks residues equivalent to cQ32 and cT67, which might act as coordination sites for the arginine. Whether a free backbone carbonyl (cV63 for *I. tartaricus*) for formation of a hydrogen bond to the γNH group is also present in the *E. coli* enzyme is unclear, but this has been speculated recently [19]. Based on these considerations, interaction of the arginine with the proton-binding site is expected to be weaker than with the Na^+ ion-binding site. A strong interaction between the binding site and the arginine is not favorable for high turnover rates, and hence the different affinities of the two enzymes for the stator arginine might explain the different translocation rates within F_0 (1000 Na^+/s versus 8000 H^+/s) [21,22]. Therefore, the incoming Na^+ ion is thought to weaken the rather strong interaction between the arginine and the binding site and to promote its loading onto the binding site, aided by the membrane potential as described previously [3]. Such a scenario is supported by the requirement of Na^+ ions for rotation, even under ATP-hydrolyzing conditions [5]. The repelled arginine is then attracted by the next incoming rotor site and displaces the Na^+ ion to form the intermediate described above. Such a concerted mechanism ensures that only small energy barriers have to be overcome during rotation in order to guarantee smooth enzyme function. According to our data, the side chain of the glutamate is not pulled towards subunit a, but is pressed inwards, which makes a large back-flipping of the acidic side chain obsolete. Such a model would also explain the earlier and so far unexplained finding that, in the *E. coli* ATP synthase, the essential cD61 on the outer helix of the c-ring can be transferred to position 24 on the inner helix with retention of activity [23]. Taking the envisaged side-chain drift of aR226 towards the P-side into account, it is tempting to speculate that, during rotation, the long side chain of aR226 oscillates like a pendulum between the binding sites of the c-ring and subunit a. Such a mechanism is favored by the highly conserved aG229, which might provide space for back pressure during rotation between two binding sites. A functional aspect of this glycine residue is anticipated but so far unexplained, as rotation during ATP hydrolysis is severely impeded ($> 90\%$ inhibition) in the corresponding mutant of the *E. coli* ATP synthase (aG213C) [9].

Possible roles for cG25 and cT67

The deficiency of the cG25I mutant in ATP synthesis demonstrates the functional importance of this

residue. To account for this, two major scenarios are possible. In the first, the *c*Y70 side chain, which is no longer hydrogen-bonded to *c*E65, could rotate into this cavity, as proposed previously [1]. This could open the binding site and an incoming Na$^+$ ion could displace the bound arginine. In the second scenario, the cavity formed by the glycines might act as vestibule for the incoming Na$^+$ ion. Free access of the cavity to the binding site would perfectly suit the requirement to allow displacement of the stator charge through the Na$^+$ ion. Again, the uncoordinated side chain of the *c*Y70 might be displaced (not into the cavity, however) and act as gate to the vestibule.

Surprisingly, the *c*T67C mutant was also unable to synthesize ATP under the conditions used. However, unlike the *c*G25I mutant, no steric reasons are assumed for this observation. One of the minimization calculations (Fig. 6D) suggests a possible role for *c*T67 as a hydrogen-accepting group for arginine (and donor for *c*E65), which would not be possible in the *c*T67C mutant. However, whether such an intermediate contribution of *c*T67 occurs during catalysis cannot be confirmed by the present data and requires further investigation.

Experimental procedures

Materials

Unless otherwise stated, chemicals were purchased from Fluka (Buchs, Switzerland).

Construction of mutants

Plasmid pItTr5His carries the whole *atp* operon (*atpIBEFHAGDC*) of *I. tartaricus* [24] with the following modifications: the start codons of *atpF* and *atpA* were changed from TTG to ATG, a *Bsu*15I single site was introduced between *atpE* and *atpF*, and a His$_{10}$ tag was fused to the N-terminus of subunit β. The endogenous cysteine at position *a*C76 of subunit *a* was then changed to alanine, resulting in plasmid pItTr6His which encodes the entire *I. tartaricus* ATP synthase with a Cys-less F$_0$ part. In this study, cysteine and other substitutions were introduced into subunits *a* and *c* on plasmid pItTr6His. *E. coli* DH5α served as host for cloning and was cultivated in LB medium supplemented with 200 μg·mL^{-1} ampicillin. Amino acid substitutions were introduced by performing a two-step PCR procedure using two oligonucleotide pairs. One pair contained the codon for the desired mutation, the sequence of the other was derived from the wild-type. The presence of the mutant codons was confirmed by automated

sequencing of the cloned DNA at Microsynth AG (Balgach, Switzerland).

Membrane preparation

Plasmids coding for cysteine-substituted *I. tartaricus* ATP synthases were expressed in the *E. coli atp* operon deletion strain DK8 [24a]. The cells were collected, washed with a buffer containing 10 mM Tris/HCl pH 8.0 and 10 mM dithiothreitol, and, if necessary, stored at −80 °C.

The cell pellet was resuspended (5 mL·g^{-1} cells, wet weight) in French press buffer I (50 mM Tris/HCl pH 8.0, 5 mM MgCl$_2$, 2 mM NaCl, 10% glycerol, 10 mM dithiothreitol, 0.1 mM diisopropylfluorophosphate, 50 μg DNase I) and disrupted by three passages through a French pressure cell. Unbroken cells and large cell debris were removed by centrifugation (8000 *g*, 4 °C, 15 min). The membranes were pelleted by ultracentrifugation (200 000 *g*, 45 min, 4 °C), and washed with 20 mL of French press buffer I containing 1 mM dithiothreitol. After centrifugation, the washed membranes were resuspended in 1 mL of assay buffer (50 mM Tris/HCl pH 8.0, 5 mM MgCl$_2$, 2 mM NaCl, 10% glycerol) for standard cross-linking assays. To determine the pH dependency of formation of *ac* cross-linking products, membrane samples were resuspended in assay buffer containing 1 mM instead of 50 mM Tris/HCl, pH 8.0. All steps were carried out at 4 °C or on ice.

Copper phenanthroline-catalyzed air oxidation of membranes

Unless otherwise noted, copper cross-linking was performed by mixing a 100 μL aliquot of membranes in assay buffer with 100 μL of CuP-solution which consisted of 10 mM *o*-phenanthroline and 3 mM CuSO$_4$ in assay buffer. To measure the influence of varying proton concentrations on the formation of *ac* cross-linking products, the pH of a 75 μL aliquot of membranes was adjusted by the addition of 25 μL MMT buffer (100 mM Mes, 100 mM Mops, 100 mM Tricine, adjusted to the desired pH with 5 M KOH). To stop the oxidation reaction, EDTA and NEM (stock solution in dimethylsulfoxide) were added to final concentrations of 15 mM each, followed by incubation for another 10 min at room temperature. In control experiments, in which NEM and EDTA were added 10 min prior to CuP, no formation of *ac* cross-linking products was observed.

Extraction of subunits *a* and *c* from oxidized membrane samples by organic solvents

The extraction of subunits *a* and *c* from oxidized membranes was performed as described previously [25]. An aliquot of 20 μL 5% acetic acid was added to 80 μL of

oxidized membranes. After addition of 1 mL of chloroform/methanol (1 : 1, v/ v) and vigorous shaking, insoluble proteins were removed by centrifugation at 15 800 *g* for 5 min. The supernatant, transferred to a new test tube, was mixed with 200 μL of 5% acetic acid. Mixing and a subsequent centrifugation step (15 800 *g*, 1 min) induced a phase separation. The lower organic phase, containing subunits *a* and *c*, was mixed with 20 μL of a 1% SDS solution, dried under vacuum and solubilized in 60 μL non-reducing 1× SDS sample buffer (50 mM Tris/HCl pH 6.8, 1% SDS, 10% glycerol, 0.1 mg·mL^{-1} bromophenol blue).

SDS–PAGE and immunoblotting

SDS–PAGE was performed under non-reducing conditions as described previously [26]. The proteins were transferred to nitrocellulose sheets (Protran nitrocellulose transfer membrane; Schleicher & Schuell BioScience GmbH, Dassel, Germany) using a semi-dry western blotting procedure as described by the manufacturer of the blotting apparatus (GE Healthcare, Glattbrugg, Switzerland). After blocking of the nitrocellulose membrane overnight with blocking buffer [1% blocking reagent (Boehringer Mannheim GmbH, Mannheim, Germany) in TTBS (20 mM Tris/HCl pH 7.5, 500 mM NaCl and 0.05% Tween-20)], it was washed twice with TTBS. The membranes were then incubated with rabbit anti-*a* or anti-*c* serum for 3 h. The anti-*a* antibody was custom-made by Eurogentec SA (Seraing, Belgium), and recognizes the *I. tartaricus* subunit *a* segment from amino acid positions 90–103, and the anti-*c* antibody was raised against the highly similar *c* subunit of *P. modestum*. Both sera were diluted 1 : 6000 in TTBS supplemented with 3% BSA. The membrane was rinsed twice with TTBS and incubated for 2 h with a 1 : 3000 dilution of alkaline phosphatase-conjugated goat anti-rabbit IgG (Bio-Rad, Hercules, CA, USA) in TTBS. Subsequently, the blots were washed first with TTBS for 2 × 5 min and then with Tris/HCl for 5 min. The alkaline phosphatase conjugate was visualized by performing a color development reaction using 5-bromo-4-chloro-3-indoyl phosphate *p*-toluidine salt and *p*-nitroblue tetrazolium chloride.

Quantification of *ac* cross-linking product formation

The developed immunoblots were scanned and the software QUANTITY ONE (Bio-Rad, Hercules, CA, USA) was applied for quantitative analysis of bands detected on the western blots as indicated in Fig. 1B. A linear dependence between the protein amount and the western blot signal was observed in the applied concentration range, as verified in a control experiment with a serial dilution of a sample.

Purification and reconstitution of recombinant ATP synthase

The protocol for His-tagged *E. coli* ATP synthase purification was used with modifications [27]. Briefly, about 5 g (wet weight) of *E. coli* DK8 cells containing heterologously expressed *I. tartaricus* ATPase were resuspended in 25 mL French press buffer II (200 mM Tris/HCl pH 7.8, 100 mM KCl, 5 mM MgCl$_2$, 0.1 mM EDTA, 2.5% glycerol, 0.1 mM diisopropylfluorophosphate, 50 μg DNase I) and disrupted in a French pressure cell. Unbroken cells and large cell debris were removed by centrifugation (8000 *g*, 10 min, 4 °C). Membranes were collected by ultracentrifugation (200 000 *g*, 45 min, 4 °C) and solubilized for 1 h at 4 °C in 20 mL extraction buffer (50 mM Tris/HCl pH 7.5, 100 mM KCl, 250 mM sucrose, 40 mM aminocaproic acid, 15 mM *p*-aminobenzamidine, 5 mM MgCl$_2$, 0.1 mM EDTA, 0.2 mM dithiothreitol, 0.8% soybean phosphatidyl choline, 1.5% octyl glucoside, 0.5% sodium cholate, 0.5% sodium deoxycholate, 2.5% glycerol and 30 mM imidazole). After centrifugation (200 000 *g*, 1 h, 4 °C), the supernatant was sterile-filtered and loaded onto a HisTrap HP 1 mL column (GE Healthcare). The column was washed with 15 mL of washing buffer (1 : 1 dilution of extraction buffer and 30 mM imidazole), and the ATPase was eluted using elution buffer (washing buffer but with 400 mM imidazole). Enzyme-containing fractions were pooled and stored in liquid nitrogen.

For reconstitution, 60 mg soybean phosphatidylcholine were homogenized in 2 mL liposome buffer (10 mM Hepes/KOH pH 6.5, 100 mM NaCl, 5 mM MgCl$_2$, 0.1 mM EDTA, 0.2 mM dithiothreitol). The suspension was sonicated on ice for 1 min using a tip-type sonicator (MSE Soniprep 150, Labtec AG, Wohlen, Switzerland). To the liposome suspension, sodium cholate (1.5% final concentration) and purified ATP synthase in a lipid : protein ratio 200 : 1 (w/w) were added. The mixture was kept for 30 min at 4 °C, and then a 500 μL sample was loaded on a PD-10 gel filtration column (GE Healthcare) equilibrated with liposome buffer. Turbid fractions were pooled and proteoliposomes collected by ultracentrifugation (200 000 *g*, 30 min, 4 °C) and suspended in 100 μL of liposome buffer.

ATP synthesis measurements

An aliquot of 250 μL sample buffer (10 mM Tris/HCl, pH 6.5, 100 mM KCl, 5 mM MgCl$_2$) was mixed with 50 μL of luciferase reagent (ATP bioluminescence assay kit CLS II, Roche Diagnostics, Rotkreuz, Switzerland) and 5 μL of liposomes. The ATP synthesis reaction was started by injection of 250 μL injector buffer (10 mM Tris/HCl pH 6.5, 10 mM potassium phosphate buffer pH 6.5, 100 mM KCl, 5 mM MgCl$_2$, 1 mM ADP, 2 μM valinomycin), and the luminescence was followed using a luminometer (Glomax, Promega,

Dübendorf, Switzerland). Control experiments were carried out as above, but in the presence of 1 μM nigericin.

Energy-minimization calculations

Energy calculations were performed using CNS 1.2 [28] on a Linux workstation using a force field with explicit hydrogens, corresponding to the files *protein-allhdg.top* and *protein-allhdg.param*. Minimization utilized the limited-memory Broyden–Fletcher–Goldfarb–Shanno method available in CNS, which was run until convergence; this usually required less than 4000 iterations. The starting structure used was the 2.4 Å X-ray structure of the *I. tartaricus c*-ring [6] with crystallographic waters removed, and residues aI225–aM231 (helix 4 of subunit a) in an ideal helical conformation placed parallel to the outer helix of the c-ring at a distance between helix axes of 12 Å. The longitudinal rotation of the model helix was such that the side chain of aR226 pointed towards and into the binding pocket of the *I. tartaricus c*-ring. Harmonic restraints were placed on the backbone atoms of the c-ring, with the intention that only the residues of the a subunit and the side chains of the c-ring should be free to move during minimization. To avoid trapping in local minima, several starting arrangements differing by minor reorientations were tried, as well as removal of the harmonic restraints on the backbone atoms around the binding pocket. Manual placement of aI225–aM231, as well as visualization of the results of energy minimization, was performed using COOT [29] and PYMOL (DeLano Scientific, Palo Alto, CA, USA).

Acknowledgements

References

1 Meier T, Morgner N, Matthies D, Pogoryelov D, Keis S, Cook GM, Dimroth P & Brutschy B (2007) A tridecameric c ring of the adenosine triphosphate (ATP) synthase from the thermoalkaliphilic *Bacillus sp.* strain TA2.A1 facilitates ATP synthesis at low electrochemical proton potential. *Mol Microbiol* **65**, 1181–1192.

2 Capaldi RA & Aggeler R (2002) Mechanism of the F_1F_0-type ATP synthase, a biological rotary motor. *Trends Biochem Sci* **27**, 154–160.

3 Dimroth P, von Ballmoos C & Meier T (2006) Catalytic and mechanical cycles in F-ATP synthases. *EMBO Rep* **7**, 276–282.

4 Greie JC, Heitkamp T & Altendorf K (2004) The transmembrane domain of subunit b of the *Escherichia coli* F_1F_0 ATP synthase is sufficient for H^+-translocating activity together with subunits a and c. *Eur J Biochem* **271**, 3036–3042.

5 Wehrle F, Kaim G & Dimroth P (2002) Molecular mechanism of the ATP synthase's F_0 motor probed by mutational analyses of subunit a. *J Mol Biol* **322**, 369–381.

6 Meier T, Polzer P, Diederichs K, Welte W & Dimroth P (2005) Structure of the rotor ring of F-type Na^+-ATPase from *Ilyobacter tartaricus*. *Science* **308**, 659–662.

7 Murata T, Yamato I, Kakinuma Y, Leslie AG & Walker JE (2005) Structure of the rotor of the V-type Na^+-ATPase from *Enterococcus hirae*. *Science* **308**, 654–659.

8 Angevine CM, Herold KA & Fillingame RH (2003) Aqueous access pathways in subunit a of rotary ATP synthase extend to both sides of the membrane. *Proc Natl Acad Sci USA* **100**, 13179–13183.

9 Angevine CM, Herold KA, Vincent OD & Fillingame RH (2007) Aqueous access pathways in ATP synthase subunit a: reactivity of cysteine substituted into transmembrane helices 1, 3 and 5. *J Biol Chem* **282**, 9001–9007.

10 Jiang W & Fillingame RH (1998) Interacting helical faces of subunits a and c in the F_1F_0 ATP synthase of *Escherichia coli* defined by disulfide cross-linking. *Proc Natl Acad Sci USA* **95**, 6607–6612.

11 Fillingame RH, Angevine CM & Dmitriev OY (2003) Mechanics of coupling proton movements to c-ring rotation in ATP synthase. *FEBS Lett* **555**, 29–34.

12 Rastogi VK & Girvin ME (1999) Structural changes linked to proton translocation by subunit c of the ATP synthase. *Nature* **402**, 263–268.

13 Nakano T, Ikegami T, Suzuki T, Yoshida M & Akutsu H (2006) A new solution structure of ATP synthase subunit c from thermophilic *Bacillus* PS3, suggesting a local conformational change for H^+-translocation. *J Mol Biol* **358**, 132–144.

14 Vincent OD, Schwem BE, Steed PR, Jiang W & Fillingame RH (2007) Fluidity of structure and swiveling of helices in the subunit c ring of *Escherichia coli* ATP synthase as revealed by cysteine–cysteine cross-linking. *J Biol Chem* **282**, 33788–33794.

15 Fraga D, Hermolin J & Fillingame RH (1994) Transmembrane helix–helix interactions in F_0 suggested by suppressor mutations to Ala24 → Asp/Asp61 → Gly mutant of ATP synthase subunit. *J Biol Chem* **269**, 2562–2567.

16 Kaim G & Dimroth P (1998) Voltage-generated torque drives the motor of the ATP synthase. *EMBO J* **17**, 5887–5895.

17 Dimroth P, von Ballmoos C, Meier T & Kaim G (2003) Electrical power fuels rotary ATP synthase. *Structure* **11**, 1469–1473.

18 Vonck J, Krug von Nidda T, Meier T, Matthey U, Mills DJ, Kühlbrandt W & Dimroth P (2002) Molecular architecture of the undecameric rotor of a bacterial Na^+-ATP synthase. *J Mol Biol* **321**, 307–316.

19 von Ballmoos C & Dimroth P (2007) Two distinct proton binding sites in the ATP synthase family. *Biochemistry* **46**, 11800–11809.

20 Kluge C & Dimroth P (1993) Kinetics of inactivation of the F_1F_0 ATPase of *Propionigenium modestum* by dicyclohexylcarbodiimide in relationship to H^+ and Na^+ concentration: probing the binding site for the coupling ions. *Biochemistry* **32**, 10378–10386.

21 Feniouk BA, Kozlova MA, Knorre DA, Cherepanov DA, Mulkidjanian AY & Junge W (2004) The proton-driven rotor of ATP synthase: ohmic conductance (10 fS), and absence of voltage gating. *Biophys J* **86**, 4094–4109.

22 Kluge C & Dimroth P (1992) Studies on Na^+ and H^+ translocation through the F_0 part of the Na^+-translocating F_1F_0 ATPase from *Propionigenium modestum*: discovery of a membrane potential dependent step. *Biochemistry* **31**, 12665–12672.

23 Miller MJ, Oldenburg M & Fillingame RH (1990) The essential carboxyl group in subunit c of the F_1F_0 ATP synthase can be moved and H^+-translocating function retained. *Proc Natl Acad Sci USA* **87**, 4900–4904.

24 Oberfeld B (2006) *F_1F_0 ATP synthase: identification of a plug within the c-ring and heterologous expression of a sodium-translocating enzyme*. PhD Thesis, ETH Zürich, Switzerland.

24a Kilonsky DJ, Brusilow WS & Simoni RD (1984) *In vivo* evidence for the role of the e subunit as an inhibitor of the proton-translocating ATPase of *Escherichia coli*. *J Bacteriol* **160**, 1055–1060.

25 von Ballmoos C (2005) *Molecular interactions along the ion pathway of the F_1F_0 ATP synthase*. PhD Thesis, ETH Zürich, Switzerland.

26 Schägger H & von Jagow G (1987) Tricine–sodium dodecyl sulfate–polyacrylamide gel electrophoresis for the separation of proteins in the range from 1 to 100 kDa. *Anal Biochem* **166**, 368–379.

27 Ishmukhametov RR, Galkin MA & Vik SB (2005) Ultrafast purification and reconstitution of His-tagged cysteine-less *Escherichia coli* F_1F_0 ATP synthase. *Biochim Biophys Acta* **1706**, 110–116.

28 Brunger AT, Adams PD, Clore GM, DeLano WL, Gros P, Grosse-Kunstleve RW, Jiang JS, Kuszewski J, Nilges M, Pannu NS *et al.* (1998) Crystallography & NMR system: a new software suite for macromolecular structure determination. *Acta Crystallogr D* **54**, 905–921.

29 Emsley P & Cowtan K (2004) Coot: model-building tools for molecular graphics. *Acta Crystallogr D* **60**, 2126–2132.

30 Laubinger W & Dimroth P (1988) Characterization of the ATP synthase of *Propionigenium modestum* as a primary sodium pump. *Biochemistry* **27**, 7531–7537.